

CIRCULATION COPY
SUBJECT TO RECALL
IN TWO WEEKS

UCRL- 84338
PREPRINT



Alfvén-Ion-Cyclotron Instability
in Mirror Machines

Duncan C. Watson

Physics of Fluids

April 21, 1980

The logo for Lawrence Livermore Laboratory, featuring a stylized 'L' and the text 'Lawrence Livermore Laboratory' in a bold, sans-serif font, all contained within a white rectangular box with a black border.

Lawrence
Livermore
Laboratory

This is a preprint of a paper intended for publication in a journal or proceedings. Since changes may be made before publication, this preprint is made available with the understanding that it will not be cited or reproduced without the permission of the author.

DISCLAIMER

This document was prepared as an account of work sponsored by an agency of the United States Government. Neither the United States Government nor the University of California nor any of their employees, makes any warranty, express or implied, or assumes any legal liability or responsibility for the accuracy, completeness, or usefulness of any information, apparatus, product, or process disclosed, or represents that its use would not infringe privately owned rights. Reference herein to any specific commercial product, process, or service by trade name, trademark, manufacturer, or otherwise, does not necessarily constitute or imply its endorsement, recommendation, or favoring by the United States Government or the University of California. The views and opinions of authors expressed herein do not necessarily state or reflect those of the United States Government or the University of California, and shall not be used for advertising or product endorsement purposes.

ALFVÉN-ION-CYCLOTRON INSTABILITY IN MIRROR MACHINES^a

Duncan C. Watson^b

Lawrence Livermore Laboratory, University of California
Livermore, CA 94550

ABSTRACT

The Alfvén-ion-cyclotron instability is studied for finite mirror-confined plasmas with high beta without field-reversal. Variation perpendicular to field-lines is modeled by an effective k_{\perp} . Variation along a representative field-line is treated using the Wentzel-Kramer-Brillouin approximation in two ways. First, the local dispersion relation is expanded about a wavenumber and frequency corresponding to absolute instability at the machine midplane. This yields a parabolic $k_{\parallel}(s)$ and a frequency correction. Second, the local dispersion relation is evaluated exactly as a function of position, and the appropriate phase-integral condition is used to fix the frequency. This condition is chosen using a generalized WKB formulation which is outlined. The two ways of obtaining the mode frequency agree closely. Stability boundaries are drawn in $\beta_{\perp} - \beta_{\parallel}$ space for two representative finite plasmas. The long thin approximation is used to model finite-beta well-deepening. For ease of computation, the bi-Maxwellian ion velocity distribution is used. At high β the stability boundaries are affected by the appearance of an additional root, with a larger parallel wavenumber and a lower frequency.

^aWork performed under the auspices of the U. S. Department of Energy by the Lawrence Livermore Laboratory under contract number W-7405-ENG-48.

^bPresent address: Rockwell International, Space Operations & Satellite Systems Division, 12214 Lakewood Blvd., Downey, CA 90241

I. INTRODUCTION

As mirror β -values increase, electromagnetic instabilities become important. Such instabilities have been extensively studied in space plasmas.¹ In this paper the Alfvén-ion-cyclotron instability^{2,3} is studied for finite mirror-confined plasmas with high beta but without field-reversal. The effects of spatial inhomogeneity are included to second order. In general, the WKB method cannot be applied in more than one dimension; therefore, variation perpendicular to field lines is modeled by an effective k_{\perp} . Variation along a representative field-line is treated using the WKB approximation in two ways. First, the wavenumber and frequency corresponding to absolute instability at the midplane are found using the Briggs-Bers criterion⁴ of a pinch-point in the complex k_{\parallel} plane. The local dispersion relation is expanded about the midplane, yielding a parabolic $k_{\parallel}(s)$ and a frequency correction as shown by Pearlstein and Berk.⁵ Second, the local dispersion relation is evaluated exactly as a function of position, assuming a parabolic magnetic well. The turning-points and Stokes' lines are found in the complex s plane. The frequency is fixed using the appropriate phase-integral condition, chosen using a generalized WKB formulation due to Berk and Sharp.⁶ The two ways of obtaining the mode frequency agree closely.

Stability boundaries are drawn in $\beta_{\perp} - \beta_{\parallel}$ space for two representative finite plasmas. Case I is a plasma of radius 15 vacuum ion Larmor radii, lying in a parabolic magnetic well whose vacuum scale length is 50 ion Larmor radii. Case II is a plasma of radius 2.7 vacuum ion Larmor radii, lying in a parabolic magnetic well whose vacuum scale length is 15 ion Larmor radii. The long thin approximation is used to model finite-beta well-deepening. For ease

of computation, the bi-Maxwellian ion velocity distribution is used. Stability decreases with increasing beta and with increasing machine size. At high beta the stability boundaries are affected by the appearance of an additional root, with a larger parallel wavenumber and a lower frequency.

II. LOCAL DISPERSION RELATION

The dispersion relation for an Alfvén-ion-cyclotron wave propagating parallel to the magnetic field may be written²

$$0 = \frac{k_{\parallel}^2 c^2}{\omega_{pi}^2} + \frac{\omega}{\omega_{ci}} + \frac{\omega}{\omega - \omega_{ci}} + \int d^3v \frac{k_{\parallel} v_{\parallel} f_{oi}}{\omega - k_{\parallel} v_{\parallel} - \omega_{ci}} \frac{\omega}{\omega - \omega_{ci}} - \int d^3v \frac{k_{\parallel} v_{\parallel}}{\omega - k_{\parallel} v_{\parallel} - \omega_{ci}} \left(v^2 \frac{\partial f_{oi}}{\partial v_{\parallel}^2} - v^2 \frac{\partial f_{oi}}{\partial v_{\perp}^2} \right). \quad (1)$$

The first term is the free-space contribution, with displacement current omitted. The second term is the electron contribution, approximated by the E X B drift. The ion contribution is split into three terms representing, respectively, the behavior of a cold fluid, the effect of non-zero temperature, and the effect of non-zero anisotropy. The Landau damping from the second ion term competes with the Landau growth from the third ion term to determine the purely temporal behavior of the instability.

Let s be the distance along a typical field-line measured from the midplane of the machine. Assume a simple bi-Maxwellian ion distribution which obeys adiabatic invariance. Neglect ambipolar potential, then

$$f_{oi}(v_{\perp}, v_{\parallel}, s) = \frac{\alpha_{\perp}(s)}{\pi} \sqrt{\frac{\alpha_{\parallel}}{\pi}} \exp \left[-\alpha_{\perp}(s) v_{\perp}^2 - \alpha_{\parallel} v_{\parallel}^2 \right] \quad (2)$$

where

$$\alpha_1(s) = \frac{B(o)}{B(s)} \alpha_1(o) + \left(1 - \frac{B(o)}{B(s)}\right) \alpha_{||} \quad (3)$$

Then, the dispersion relation (1) reduces to³

$$0 = D_{LL}(k_{||}, s, \omega) \equiv \frac{k_{||}^2 c^2}{\omega_{pi}^2(s)} + \frac{\omega}{\omega_{ci}(s)} + \frac{\omega}{\omega - \omega_{ci}(s)} \\ + \frac{1}{2} \left[\frac{\omega}{\omega - \omega_{ci}(s)} - \left(\frac{\alpha_{||}}{\alpha_1(s)} - 1 \right) \right] z' \left(\frac{\omega - \omega_{ci}(s)}{k_{||} \sqrt{\alpha_{||}}} \right) \quad (4)$$

where

$$\omega_{pi}^2(s) = \omega_{pi}^2(o) \alpha_1(o) / \alpha_1(s) \quad (5)$$

We assume that a transverse mode pattern exists which can be modeled as having a half-wavelength within the diameter of the plasma at the midplane. Thus, at the midplane,

$$x \equiv \frac{k_{||}^2 a_{il}^2}{2} = \frac{\pi^2}{8} \frac{a_{il}^2}{R_p^2} = \frac{\pi^2}{8} \frac{a_{ilv}^2}{R_p^2 (1 - \beta_{lv})} \quad (6)$$

where the subscript v denotes quantities defined with respect to the vacuum field, and the long thin approximation has been used. We further assume that the mode pattern is tied to the field lines, and neglect quadrupole effects. Strictly speaking, this introduces a variation of the parameter

$$x(s) \equiv \frac{k_{||}^2(s) a_{il}^2(s)}{2} = x(o) \frac{B(o)}{B(s)} \frac{\alpha_1(o)}{\alpha_1(s)} \quad (7)$$

along a field line, but this will be neglected.

The determinant of the dispersion tensor now serves as the local dispersion function. The electrons are cool and the frequency is low; thus, the parallel electric field is shorted out and coupling to the right-hand polarized mode is the only coupling that need be included. The local dispersion relation in an obvious notation is

$$0 = D_{\ell\ell} - \frac{D_{\ell r} D_{r\ell}}{D_{rr}} \quad (8)$$

Explicitly,

$$\begin{aligned} 0 = D(k_{\parallel}, \omega, s) \equiv & \left(\frac{k_{\parallel}^2 c^2}{\omega_{pi}^2} + \frac{k_{\perp}^2 c^2}{2\omega_{pi}^2} + \frac{\omega}{\omega_{ci}} + \sum_{n=-\infty}^{\infty} X_n^{\ell\ell} Z_n \right) \\ & - \left(\frac{k_{\perp}^2 c^2}{2\omega_{pi}^2} - \sum_{n=-\infty}^{\infty} X_n^{\ell r} Z_n \right)^2 \left(\frac{k_{\parallel}^2 c^2}{\omega_{pi}^2} + \frac{k_{\perp}^2 c^2}{2\omega_{pi}^2} - \frac{\omega}{\omega_{ci}} \right. \\ & \left. + \sum_{n=-\infty}^{\infty} X_n^{rr} Z_n \right)^{-1} \quad (9) \end{aligned}$$

where $\omega_{pi}^2(s)$ is given by (5), x is given by (6), and

$$X_n^{\ell\ell} = -\left(\frac{x}{2} - n\right) \Gamma_{n-1} + (x-n) \Gamma_n - \frac{x}{2} \Gamma_{n+1} \quad (10)$$

$$X_n^{rr} = -\frac{x}{2} \Gamma_{n-1} + (x+n) \Gamma_n - \left(\frac{x}{2} + n\right) \Gamma_{n+1} \quad (11)$$

$$X_n^{\ell r} = \frac{x}{2} \Gamma_{n-1} - x \Gamma_n + \frac{x}{2} \Gamma_{n+1} \quad (12)$$

$$\Gamma_n = I_n(x) e^{-x}, \quad (13)$$

$$z_n = \frac{\omega}{\omega - n\omega_{ci}} + \frac{1}{2} \left[\frac{\omega}{\omega - n\omega_{ci}} - \left(\frac{\alpha_{\parallel}}{\alpha_{\perp}} - 1 \right) \right] z' \frac{\omega - n\omega_{ci}}{k_{\parallel} / \sqrt{\alpha_{\parallel}}} \quad (14)$$

The transverse wavevector in (9) is treated as a parameter and the parallel mode variation treated by one of the two methods to which we now turn.

III. EXPANSION ABOUT ABSOLUTE INSTABILITY

The Briggs-Bers criterion for absolute instability in a homogeneous medium³ is that there exist a k_o , ω_o such that

$$D(k_o, \omega_o) = 0, \quad (15)$$

$$(\partial D / \partial k) \big|_{k_o, \omega_o} = 0, \quad (16)$$

and such that the coincident roots $k(\omega_o)$ migrate to opposite sides of the real k axis as $\omega_i \rightarrow +\infty$.

One way to deal with the inhomogeneous problem is as follows.⁴ Suppose that one can find an "absolute instability in the midplane plasma," or more strictly that one can find a $k_{\parallel o}$, ω_o such that

$$D(k_{\parallel o}, 0, \omega_o) = 0, \quad (17)$$

$$\left[\partial D(k_{\parallel}, 0, \omega_o) / \partial k_{\parallel} \right]_{k_{\parallel o}} = 0, \quad (18)$$

where the dispersion function is given by (9). Expanding D about $(k_{\parallel o}, \omega_o, 0)$

one obtains an s dependence for k_{\parallel} , whose form depends on the assumed frequency-shift $\Delta\omega$:

$$0 = D(k_{\parallel 0} + \Delta k_{\parallel}, s, \omega_0 + \Delta\omega), \quad (19)$$

$$0 = \frac{(\Delta k_{\parallel})^2}{2} \frac{\partial^2 D}{\partial k^2} + \Delta\omega \frac{\partial D}{\partial \omega} + \frac{s^2}{2} \frac{\partial^2 D}{\partial s^2}. \quad (20)$$

The phase-integral method will be discussed in detail in Section IV. Here, we use the fact that, under certain conditions, a spatially-confined mode exists when

$$(2n + 1)\pi + \int_{-s_t}^{s_t} ds \left[k_{\parallel}^+(s) - k_{\parallel}^-(s) \right], \quad (21)$$

where the roots k_{\parallel}^+ , k_{\parallel}^- coincide at $s = \pm s_t$, the so-called turning-points.

Using the local dispersion relation (20) one deduces that a spatially-confined mode exists when

$$\Delta\omega = - \frac{2n+1}{2(\partial D / \partial \omega)} \left(\frac{\partial^2 D}{\partial s^2} \frac{\partial^2 D}{\partial k_{\parallel}^2} \right)^{1/2}, \quad (22)$$

where all derivatives are evaluated at $(k_{\parallel 0}, \omega_0, 0)$. This is the Pearlstein-Berk estimate⁵ of the finite-length frequency-shift. The sign of the square root is chosen in accord with the exact phase-integral solution in Section IV.

Figure 7 shows the stability boundaries in $\beta_{\perp} - \beta_{\parallel}$ parameter space for two different-sized plasmas. Case I is a plasma of radius 15 vacuum ion Larmor radii, lying in a parabolic magnetic well whose vacuum scale length is

50 ion Larmor radii. Case II is a plasma of radius 2.7 Larmor radii, in a well of scale length 15 Larmor radii. In both cases the long thin approximation is used to estimate the finite- β magnetic-field depression. Figure 1 shows for comparison the absolute stability boundaries for infinite-length systems, i.e., $\Delta\omega = 0$.

Topology checks in the complex k plane are carried out at the parameter points indicated by circles in Fig. 1. For both case I and case II, the kink in the stability boundary is associated with the existence of two saddle-points satisfying (17) and (18). The one with the higher growth-rate determines the boundary, as long as it is a true pinch-point. The topology checks for case I are displayed in Figs. 2 - 4, for case II in Figs. 5 and 6. In each case the "usual" saddle point is the one determining stability at low and moderate β_1 . The arrows indicate the migration of the k roots as $\omega_1 \rightarrow +\infty$. The frequency is normalized to the actual midplane ion gyrofrequency. The wavenumber is normalized to the actual midplane ion gyroradius, defined in terms of $2\langle v^2 \rangle / 3$ rather than $\langle v_1^2 \rangle$.

Topology checks for the finite-length systems are carried out at the parameter points indicated by circles in Fig. 7. For case I the stability boundary is smooth. The "usual" saddle-point displays the same behavior at high β_1 that the "other" saddle-point displayed in the infinite-length system. For case II the boundary is qualitatively similar to that with $\Delta\omega = 0$. The k -plane topology checks for case I are displayed in Figs. 8 and 9, for case II in Figs. 10 and 11. The frequency is normalized to the actual depressed-field midplane ion gyrofrequency. The wavenumber is normalized to the actual midplane gyroradius, defined in terms of $2\langle v^2 \rangle / 3$.

For case I it is found that only the $\ell = 0, \pm 1$ gyroharmonics need be included in the computations. For case II the $\ell = \pm 2$ must be included also. For case II the factor $(1 - \beta_{1v})$ in the denominator of (5) is replaced by $(1 - \beta_{1v})^{1/2}$. This is an attempt to allow for the narrow, sloping shape of the $\beta_1(r)$ dependence in the case I plasma, as distinct from the flat-topped $\beta_1(r)$ dependence expected in case II.

IV. GENERALIZED WKB THEORY

We use a generalized WKB method due to Berk and Sharp⁶. This method can be used for integral equations. The turning points are not restricted to $k = 0$. The method constitutes the extension of Briggs-Bers analysis to finite systems, and provides complex eigenfrequencies and eigenmodes.

Given an integral equation

$$0 = \int \tilde{D} \left(z - Z, \frac{z + Z}{2}, \omega \right) E(Z) dZ \quad (23)$$

one obtains a solution in terms of a superposition of waves

$$E(s) = \sum_n c_n \left(\frac{\partial D(k_n, s, \omega)}{k} \right)^{-1/2} \exp \left[i \int_0^s k_n(\omega, s') ds' - i\omega t \right] \quad (24)$$

Here, the c_n are constants and the k_n satisfy the local dispersion relation

$$0 = D(k_n, s, \omega) \equiv \int_{-\infty}^{\infty} \tilde{D}(y, s, \omega) e^{ik_n y} dy \quad (25)$$

The physical interpretation is that a system can support many waves each characterized by a particular $k_n(s, \omega)$. Each wave has a conserved action-flow

$$A_n(z) = |E_n^2| \left[-\partial D(k_n, s, \omega) / \partial k \right] \quad (26)$$

This may be written as the product of action density and group velocity

$$A_n(z) = |E_n^2| \partial D / \partial \omega \left(\frac{\partial D / \partial k_n}{\partial D / \partial \omega} \right) \quad (27)$$

A physical question arises: if each wave carries action right through the system, how can a confined mode ever occur? The answer is that a confined mode can only occur if one wave couples to another wave with an oppositely directed action flow. Waves can couple together linearly only if they have the same frequency and wavenumber. Points at which two different waves have the same wavenumber are called turning-points; at such points $\partial D / \partial k$ is zero. The procedure for determining mode structure will now be described. For the remainder of this section z replaces s and the subscript ℓ does not mean left-handed.

The first step is to locate all relevant turning-points and locate the intercepts on the real z axis of all the Stokes' lines emanating from those turning-points.

The second step is to decide which roots $k_n(z)$ yield waves that can form part of the solution as $z \rightarrow +\infty$, and which roots are good as $z \rightarrow -\infty$.

The third step is to continue the solutions inward from $\pm\infty$, using the following formula for coupling of waves near a turning-point. Let z_t be a turning-point where $k_h = k_\ell$. Let z_s be the intercept on the real axis of a Stokes' line emanating from z_t , and let k_h be there dominant with

respect to z_t , i.e., let

$$\exp \left\{ i \int_{z_t}^{z_s} [k_h(z') - k_\ell(z')] dz' \right\}$$

be exponentially large. Then, the wave

$$E(z) = c_h \left(\partial D / \partial k_h \right)^{-1/2} \exp \left(i \int_0^z k_h dz' \right) \quad (28)$$

on one side of the Stokes' line has a continuation

$$\begin{aligned} E(z) = & c_h \left(\partial D / \partial k_h \right)^{-1/2} \exp \left(i \int_0^z k_h dz' \right) \\ & + c_h \left(\partial D / \partial k \right)^{-1/2} \exp \left(i \int_0^{z_t} k_h dz' + i \int_{z_t}^z k_\ell dz' \right) \end{aligned} \quad (29)$$

on the other side. The sign of the square root is chosen so that near z_t

$$\left(\partial D / \partial k \right)^{-1/2} \sim \pm i \left(\partial D / \partial k_h \right)^{-1/2} \quad (30)$$

where the plus sign is chosen if the continuation is made in a clockwise direction about z_t . This is consistent with Furry.⁷ Subdominant waves are continued across Stokes' lines unaltered.

The fourth step is to compare coefficients of the various waves after the two solutions have been continued from $\pm\infty$ to some common meeting point, say the origin. This yields a phase-integral condition which constitutes the global dispersion relation for the finite system in question.

Figure 12 is an example. The turning-points are labeled by the k roots which coincide there. It is left as a simple exercise for the reader to show that the phase-integral condition is

$$-1 = \exp \left[i \int_{\hat{z}_{h\ell}}^{z_{h\ell}} dz (k_{\ell} - k_h) \right] + \exp \left[i \int_{\hat{z}_{hm}}^{z_{hm}} dz (k_m - k_h) \right] \quad (31)$$

provided that the allowable k roots at $z = \pm\infty$ are as indicated, and provided that k_h is dominant with respect to $\hat{z}_{h\ell}$ and \hat{z}_{hm} , subdominant with respect to $z_{h\ell}$ and z_{hm} . It is not necessary to assume symmetry of the system. Even if the system is symmetric, i.e.,

$$k_n(z) = k_n(-z) \quad , \quad (32)$$

$$\hat{z}_{ab} = -z_{ab} \quad . \quad (33)$$

Figure 12 makes it clear that the mode pattern need have no definite symmetry. Only under combined space and time reversal does the mode necessarily go into another good eigenmode.

Figure 13 shows the stability boundary in $\beta_{\perp} - \beta_{\parallel}$ space for the case I plasma described in Sec. II. This boundary differs only slightly from that shown in Fig. 7. The Pearlstein-Berk formula (22) yields, for case I, a result very close to that obtained by using the exact phase-integral formula (31).

The z -plane Stokes' line diagrams are shown in Figs. 14 - 16. The frequency and wavenumber are normalized to the actual midplane ion gyrofrequency and gyroradius, with the latter defined by $2 \langle v^2 \rangle / 3$. The dashed lines are Stokes lines, the wavy lines anti-Stokes lines. Such lines emanating from different turning-points may cross since they are level-lines of different quantities. The signs of the group velocities' real parts are shown in parentheses.

The wiggle in the stability boundary of Fig. 13 is associated with the transition from a phase integral relation determined mainly by the turning-points $\pm z_1$ to a phase-integral relation determined mainly by the turning-points $\pm z_2$. In terms of Eq. 31, the wiggle in the boundary of Fig. 13 occurs because at lower β_1 the second term on the right is exponentially small, whereas at higher β_1 the first term on the right is exponentially small.

The Stokes diagram (12) and associated phase-integral formula (31) are correct for this problem. This is obvious from an inspection of Figs. 14 - 16, with the possible exception of the choice of the root k_ℓ as representing a good solution as $z \rightarrow +\infty$. Even though k_ℓ may have a small negative imaginary part at finite z , the fact that it represents an outgoing wave ensures that the choice is correct as shown.

V. ACKNOWLEDGMENTS

First and foremost I acknowledge the help of L. Donald Pearlstein, who suggested the problem and provided valuable guidance. Second, I acknowledge many hours of fruitful discussion with Herbert L. Berk and William S. Sharp on the formulation and application of the generalized WKB theory. Finally, I acknowledge the help of Linda L. Lodestro and William S. Sharp, whose computer programs, after some adaptation, generated the results of Secs. III and IV, respectively.

APPENDIX A

EXPLICIT INTEGRO-DIFFERENTIAL EQUATION AND EXACT LOCAL DISPERSION RELATION

This appendix is restricted to the case of parallel propagation. The integro-differential equation describing Alfvén-ion-cyclotron modes confined by a magnetic well is exhibited. The ion distribution function and the shape of the well are arbitrary. The symmetry of the kernel is shown. The doubly-Fourier-transformed kernel is displayed, for future use in exact spatial eigenmode calculations. The singly-Fourier-transformed kernel, namely, the local dispersion relation (25), is displayed. It is shown that the latter reduces to the usual homogeneous-plasma dispersion relation for growth rates greater than a representative bounce-frequency.

Consider a left-hand polarized disturbance propagating along the axes of an axisymmetric mirror machine. The linearized Vlasov equation describing this disturbance, including the effect of fieldline convergence, is⁸

$$\begin{aligned}
 (\Omega - \omega) f_{\ell} - i v_{\parallel} \frac{\partial f_{\ell}}{\partial z} - i v_{\perp} \frac{\Omega'}{2\Omega} \left(v_{\parallel} \frac{\partial f_{\ell}}{\partial v_{\perp}} - v_{\perp} \frac{\partial f_{\ell}}{\partial v_{\parallel}} \right) \\
 = \frac{iq}{m} E_{\ell} \frac{\partial f_o}{\partial v_{\perp}} - \frac{q}{m\omega} \left(\frac{\partial E_{\ell}}{\partial z} - \frac{\Omega'}{2\Omega} E_{\ell} \right) \left(v_{\parallel} \frac{\partial f_o}{\partial v_{\perp}} - v_{\perp} \frac{\partial f_o}{\partial v_{\parallel}} \right) \quad . \quad (A1)
 \end{aligned}$$

Here, Ω is the ion cyclotron frequency, a prime denotes the derivative with respect to z , z is the distance along the axis measured from the midplane,

$$f_1(v_x, v_y, v_z, z) = e^{-i\phi} f_{\ell}(v_{\perp}, v_{\parallel}, z) \quad , \quad (A2)$$

$$\begin{pmatrix} v_x \\ v_y \end{pmatrix} = \begin{pmatrix} \cos \phi \\ \sin \phi \end{pmatrix} v_{\perp} , \quad (\text{A3})$$

and

$$\vec{E}_1(z) = (1, -i, 0) E_{\ell}(z) . \quad (\text{A4})$$

Assuming adiabatic invariance and defining

$$\epsilon = v^2 , \quad (\text{A5})$$

$$\mu = v_{\perp}^2 / b , \quad (\text{A6})$$

$$b(z) = B_0(z) / B_0(0) , \quad (\text{A7})$$

one may write (34) in the form

$$\begin{aligned} i(\Omega - \omega) f_{\ell} + \frac{df_{\ell}}{d\tau} = & - \frac{2q}{m} \left\{ \sqrt{\mu} [b(\tau)]^{1/2} \frac{\partial f_o}{\partial \epsilon} + \frac{1}{[b(\tau)]^{1/2}} \frac{\partial f_o}{\partial \mu} \right\} E_{\ell}(\tau) \\ & - \frac{2iq}{m} \sqrt{\mu} \frac{\partial f_o}{\partial \mu} \frac{d}{d\tau} \frac{E_{\ell}(\tau)}{[b(\tau)]^{1/2}} , \end{aligned} \quad (\text{A8})$$

where

$$z = z(\tau) , \quad (\text{A9})$$

$$v_{\parallel} = dz/d\tau . \quad (\text{A10})$$

parameterizes the unperturbed orbit. Using an integrating factor and integrating by parts one obtains, taking causality into account,

$$\begin{aligned}
 f_{\ell}(\epsilon, \mu, \sigma) = & \frac{2iq}{m} \sqrt{\mu} \frac{\partial f_o}{\partial \mu} \frac{E_{\ell}(\sigma)}{[b(\sigma)]^{1/2}} \\
 & - \frac{2q}{m} \sqrt{\mu} \left[\frac{\partial f_o}{\partial \mu}(\sigma) + \frac{\partial f_o}{\partial \epsilon} \omega \right] \int_{-\infty}^{\sigma} d\tau E_{\ell}(\tau) [b(\tau)]^{1/2} \\
 & \exp \left\{ -i \int_{\tau}^{\sigma} d\rho [\Omega(\rho) - \omega] \right\} .
 \end{aligned} \tag{A11}$$

The left-hand-polarized current, including the contribution from the cold electrons, is

$$J_{\ell}(z) = \frac{q}{2} \int d^3v v_{\perp} f_{\ell}(v_{\perp}, v_{\parallel}, z) + \frac{i\epsilon_o \omega^2(z)}{|\omega_{ce}|} E_{\ell}(z) . \tag{A12}$$

Substitution of (A11) into (A12) yields

$$\begin{aligned}
 J_{\ell}(z) = & i\epsilon_o \omega_{pi}^2(z) \left(\frac{1}{\Omega(z)} + \frac{1}{\omega} + \frac{1}{\omega} \int d^3v v_{\perp}^2 \frac{\partial F_o(z)}{\partial v_{\parallel}^2} \right) \\
 & + \frac{q\pi}{4} b^{3/2}(z) \int_0^{\infty} d\mu \sqrt{\mu} \int_{\mu b(z)} d\epsilon \frac{f_{\ell g}(\epsilon, \mu, \hat{\sigma})}{[\epsilon - \mu b(z)]^{1/2}}
 \end{aligned} \tag{A13}$$

Here, F_o is the local ion distribution function normalized to the local plasma density. The function $f_{\ell g}$ is the non-local part of f_{ℓ} and is summed over the two values of $\hat{\sigma}$ satisfying

$$z = z(\hat{\sigma}) . \tag{A14}$$

The integro-differential equation obeyed by the electric field, including the effect of wavefront curvature, is⁸

$$0 = \frac{c^2}{\omega^2} \left[\left(\frac{\partial}{\partial z} - \frac{3\Omega'}{2\Omega} \right) \left(\frac{\partial}{\partial z} + \frac{\Omega'}{2\Omega} \right) + \frac{7}{8} \left(\frac{\Omega'}{\Omega} \right)^2 \right] \times E_\ell(z) + E_\ell(z) + \frac{iJ_\ell(z)}{\epsilon_0 \omega} \quad (A15)$$

Substitution of (A11) and (A13) into (A15), and division by $b(z)$ yields

$$0 = \frac{c^2}{\omega^2} \left[\left[\Omega(z) \right]^{1/2} \frac{\partial}{\partial z} \frac{\Omega(o)}{\Omega^2(z)} \frac{\partial}{\partial z} \left[\Omega(z) \right]^{1/2} + \frac{7}{8} \frac{\Omega'^2(z) \Omega(o)}{\Omega^3(z)} \right] E_\ell(z) + \frac{\Omega(o)}{\Omega(z)} E_\ell(z) - \frac{\Omega(o)}{\Omega(z)} \frac{\omega_{pi}^2(z)}{\omega^2} \left[\frac{\omega}{\Omega(z)} + 1 + \int d^3 v_1 v^2 \frac{\partial F_o(z)}{\partial v_{||}^2} \right] E_\ell(z) - \frac{\pi i \omega_{pi}^2(o)}{4\omega^2} \left[b(z) \right]^{1/2} \int_0^\infty d\mu \mu \int_{\mu b(z)}^\infty \frac{d\epsilon}{\left[\epsilon - \mu b(z) \right]^{1/2}} \left[\frac{\partial f_o}{\partial \mu} \Omega(o) + \frac{\partial f_o}{\partial \epsilon} \omega \right] \int_{-\infty}^{\hat{\sigma}} d\tau E_\ell(\tau) \sqrt{b(\tau)} \exp \left\{ -i \int_\tau^{\hat{\sigma}} d\rho \left[\Omega(\rho) - \omega \right] \right\} \quad (A16)$$

where the integral is summed over the two values of $\hat{\sigma}$ satisfying (A14).

Schematically,

$$0 = \int \tilde{D}_\ell(z, Z) E_\ell(Z) dZ \quad (A17)$$

The kernel of (A16) is symmetric. This is demonstrated by taking the Fourier transform in both spatial variables.

$$\hat{D}_\ell(k, K) = \frac{1}{2\pi} \int dz \int \exp(-ikz + iKZ) \hat{D}_\ell(z, Z) \quad (A18)$$

$$\begin{aligned} \hat{D}_\ell(k, K) = & \frac{1}{2\pi} \int_{-\infty}^{\infty} \frac{dz}{b(z)} \exp[i(K-k)z] \left[\frac{7}{8} \frac{c^2}{\omega^2} \frac{\Omega'^2(z)}{\Omega^2(z)} \right. \\ & + \frac{1}{4} \frac{c^2}{\omega^2} \frac{[2ik\Omega(z) - \Omega'(z)][2iK\Omega(z) + \Omega'(z)]}{\Omega^2(z)} + 1 \\ & - \frac{\omega^2 p_i(z)}{2} \left(\frac{\omega}{\Omega(z)} + 1 + \int d^3v v_\perp^2 \frac{\partial F_o(z)}{\partial v_\parallel^2} \right) \Big] \\ & - \frac{i\omega^2 p_i(o)}{4\omega^2} \int_0^\infty d\mu \mu \int_\mu^\infty d\epsilon \left[\frac{\partial F_o}{\partial \mu} \Omega(o) + \frac{\partial F_o}{\partial \epsilon} \omega \right] \\ & \int_{-T/2}^{T/2} d\sigma \int_{-\infty}^\sigma d\tau [b(\sigma)]^{1/2} [b(\tau)]^{1/2} \\ & \exp[-ikz(\sigma) + iKZ(\tau)] \exp \left\{ -i \int_\tau^\sigma d\rho [\Omega(\rho) - \omega] \right\}, \quad (A19) \end{aligned}$$

where $T = T(\epsilon, \mu)$ is the orbital period and the origin of σ is arbitrary. The Hermitian nature of \hat{D}_ℓ becomes clear by inspection upon changing the variables and limits of integration.

$$\begin{aligned}
 \hat{D}_\ell(k, K) = & \frac{1}{2\pi} \int_{-\infty}^{\infty} \frac{dz}{b(z)} \exp[i(k-K)z] \left[\frac{7}{8} \frac{c^2}{\omega^2} \frac{\Omega'^2(z)}{\Omega^2(z)} \right. \\
 & + \frac{1}{4} \frac{c^2}{\omega^2} \frac{[2ik\Omega(z) - \Omega'(z)][2iK\Omega(z) + \Omega'(z)]}{\Omega^2(z)} + 1 \\
 & - \frac{\omega^2}{\omega^2} \frac{pi(z)}{\Omega^2(z)} \left(\frac{\omega}{\Omega(z)} + 1 + \int d^3v v^2 \frac{\partial F_o(z)}{\partial v_{||}^2} \right) \Bigg] \\
 & - \frac{\omega^2}{4\omega^2} \frac{pi(o)}{\Omega^2(o)} \int_0^\infty d\mu \mu \int_\mu^\infty d\epsilon \left[\frac{\partial f_o}{\partial \mu} \Omega(o) + \frac{\partial f_o}{\partial \epsilon} \omega \right] \left(\sin \left\{ \int_0^T \right. \right. \\
 & \left. \left. d\rho [\Omega(\rho) - \omega] \right\} \right)^{-1} \int_{-T/2}^{T/2} d\alpha \int_{-T/2}^{T/2} d\beta [b(\alpha - \beta)]^{1/2} [b(\alpha + \beta)]^{1/2} \\
 & \exp [-ikz(\alpha - \beta) + iKz(\alpha + \beta)] \exp \left\{ i \int_{\alpha - \beta}^{\alpha + \beta} d\rho [\Omega(\rho) - \omega] \right\}
 \end{aligned} \tag{A20}$$

The kernel D is Hermitian even though the magnetic well need not be spatially symmetric. The form (A20) may find use in exact eigenmode calculations of the type already performed for the electrostatic well by Rognlien and Watson.⁹

The local dispersion function (25) may be written

$$D_\ell(p, s) = b(s) \int dz \int dZ \ell^{-ipz} \ell^{ipZ} \tilde{D}_\ell(z, Z) \delta(s - \frac{z + Z}{2}) \tag{A21}$$

where the factor b(s) is inserted for convenience. Comparison with (A18) and (A20) immediately yields

$$\begin{aligned}
 D_{\ell}(p, s) = & \frac{c^2}{\omega^2} \left(-p^2 + \frac{3}{4} \frac{\Omega''(s)}{\Omega(s)} - \frac{7}{8} \frac{\Omega'^2(s)}{\Omega^2(s)} \right) + 1 \\
 & - \frac{\omega^2 p_i^2(s)}{2} \left(\frac{\omega}{\Omega(s)} + 1 + \int d^3v v_1^2 \frac{\partial F_o(s)}{\partial v_{\parallel}^2} \right) \\
 & - \frac{i\pi\omega^2 p_i^2(o)}{2^2} \int_0^{\infty} d\mu \mu b(s) \int_{\mu b(s)}^{\infty} d\epsilon \left[\frac{\partial f_o}{\partial \mu} \Omega(o) + \frac{\partial f_o}{\partial \epsilon} \omega \right] \int_{-T/2}^{T/2} d\sigma \\
 & \int_{-\infty}^{\sigma} d\tau [b(\sigma)]^{1/2} [b(\tau)]^{1/2} \exp [-ipz(\sigma) + ipZ(\tau)] \\
 & \exp \left\{ -i \int_{\tau}^{\sigma} d\rho [\Omega(\rho) - \omega] \right\} \delta \left\{ s - \left[\frac{z(\sigma) + Z(\tau)}{2} \right] \right\} \quad (A22)
 \end{aligned}$$

where z and Z are functions of their orbital-parameter arguments.

The local dispersion function (A22) reduces correctly to the homogeneous dispersion function (1) in the limit of large machines and strong growth. The gradient terms in the free-space contribution may be neglected when the wavelength is much shorter than the magnetic well scale length. The closure of the orbits may be neglected when the growth rate is much greater than the bounce frequency of most particles; this allows one to expand the orbital functions z, Z in (55) about $\sigma = \tau = \theta$, where θ is a value of the orbital parameter corresponding to s . The approximate local dispersion function is then

$$\begin{aligned}
 D_{\ell}(p, s) = & -\frac{p_c^2}{\omega^2} + 1 - \frac{\omega^2 p_i(s)}{\omega^2} \left(\frac{\omega}{\Omega(s)} + 1 + \int d^3v v_{\perp}^2 \frac{\partial F_o(s)}{\partial v_{\parallel}^2} \right) \\
 & - \frac{i\pi\omega^2 p_i(o)}{2} \int_0^{\infty} d\mu \mu b^2(s) \int_{\mu b(s)}^{\infty} d\epsilon \left[\frac{\partial f_o}{\partial \mu} \Omega(o) + \frac{\partial f_o}{\partial \epsilon} \omega \right] \\
 & \int_{-\infty}^{\infty} d\sigma \int_{-\infty}^{\infty} d\tau \exp \left[i\rho(\tau-\sigma) \frac{ds}{d\theta} \right] \exp \left\{ i(\tau-\sigma) [\Omega(s) - \omega] \right\} \\
 & \delta \left[\frac{ds}{d\theta} \left(\theta - \frac{\sigma + \tau}{2} \right) \right] , \tag{A23}
 \end{aligned}$$

where the integral is understood to be summed over the two possible values of θ .

Carrying out the orbital integrations

$$\begin{aligned}
 D_{\ell}(p, s) = & -\frac{p_c^2}{\omega^2} + 1 - \frac{\omega^2 p_i(s)}{\omega^2} \left(\frac{\omega}{\Omega(s)} + 1 + \int d^3v v_{\perp}^2 \frac{\partial F_o(s)}{\partial v_{\parallel}^2} \right) \\
 & + \frac{\pi\omega^2 p_i(o)}{2\omega^2} \int_0^{\infty} d\mu \mu b^2(s) \int_{\mu b(s)}^{\infty} \frac{d\epsilon}{|ds/d\theta|} \\
 & \left[\frac{\partial f_o}{\partial \mu} \Omega(o) + \frac{\partial f_o}{\partial \epsilon} \omega \right] \left[\omega - \Omega(s) - \rho \frac{ds}{d\theta} \right]^{-1} \tag{A24}
 \end{aligned}$$

Identifying $d\theta/ds$ as v_{\parallel} and μb as v_{\perp}^2 one recovers

$$D_{\ell}(p,s) = -\frac{p_c^2}{\omega^2} + 1 - \frac{\omega_{pi}^2(s)}{\omega^2} \left(\frac{\omega}{\Omega(s)} + 1 \right) \\ + \frac{\omega_{pi}^2(s)}{\omega^2} \int d^3v \frac{\rho v_{\parallel} v_{\perp}^2 \frac{\partial F_o}{\partial v_{\parallel}} - \Omega(s) F_o}{\omega - \Omega(s) - \rho v_{\parallel}}, \quad (A25)$$

which is the local parallel-propagation dispersion function (1).

REFERENCES

1. F. V. Coroniti and S. Wandzura, *Plane. and Space Sci.* 23, 123 (1975).
2. J. G. Cordey and R. J. Hastie, *Phys. Fluids* 15, 2291 (1972).
3. R. C. Davidson and J. M. Ogden, *Phys. Fluids* 18, 1045 (1975).
4. R. J. Briggs, Electron-Stream Interactions with Plasmas, (M.I.T. Press, Cambridge, 1964).
5. H. L. Berk, T. K. Fowler, L. D. Pearlstein, R. F. Post, J. D. Callen, W. C. Horton, and M. N. Rosenbluth, in Proceedings of the Conference on Plasma Physics and Controlled Nuclear Fusion (International Atomic Energy Agency, Vienna, 1969) Vol. II, p. 151.
6. W. L. Sharp and H. L. Berk, *Bull. Am. Phys. Soc.* 23, 826 (1978).
7. W. H. Furry, *Phys. Rev.* 71, 360 (1947).
8. D. C. Watson, R. J. Fateman and D. E. Baldwin, *Phys. Fluids* 21, 1657 (1978).
9. T. D. Rognlien and D. C. Watson, *Phys. Fluids* 22, 1958 (1979).

FIGURE CAPTIONS

- Figure 1 Absolute stability boundaries in $\beta_{\perp} - \beta_{\parallel}$ space for bi-Maxwellian ion distribution, infinite-length system. Briggs-Bers criterion, case I: $R_p = 15 \rho_{iv}$, case II: $R_p = 2.7 \rho_{iv}$. Topology checks marked by circles.
- Figure 2 k plane, case I. $\beta_{\perp} = 0.86$, $\beta_{\parallel} = 0.55$.
- Figure 3 k plane, case I. $\beta_{\perp} = 0.94$, $\beta_{\parallel} = 0.61$.
- Figure 4 k plane, case I. $\beta_{\perp} = 0.97$, $\beta_{\parallel} = 0.62$.
- Figure 5 k plane, case II. $\beta_{\perp} = 0.96$, $\beta_{\parallel} = 0.36$.
- Figure 6 k plane, case II. $\beta_{\perp} = 0.98$, $\beta_{\parallel} = 0.44$.
- Figure 7 Stability boundaries in $\beta_{\perp} - \beta_{\parallel}$ space for bi-Maxwellian ion distribution in mirror with 2:1 vacuum mirror ratio. Briggs-Bers criterion with Pearlstein Berk correction. Case I: $R_p = 15 \rho_{iv}$, $L = 50 \rho_{iv}$. Case II: $R_p = 2.7 \rho_{iv}$, $L = 15 \rho_{iv}$. Topology checks marked by circles.
- Figure 8 k plane, case I. $\beta_{\perp} = 0.904$, $\beta_{\parallel} = 0.520$.
- Figure 9 k plane, case I. $\beta_{\perp} = 0.980$, $\beta_{\parallel} = 0.536$.
- Figure 10 k plane, case II. $\beta_{\perp} = 0.90$, $\beta_{\parallel} = 0.06$.
- Figure 11 k plane, case II. $\beta_{\perp} = 0.94$, $\beta_{\parallel} = 0.064$.
- Figure 12 Description of confined mode using turning-points and Stokes' lines in the complex z plane.
- Figure 13 Stability boundary in $\beta_{\perp} - \beta_{\parallel}$ space for bi-Maxwellian ion distribution in mirror with 2:1 vacuum mirror ratio. Two-turning-point-pair phase-integral condition. Case I: $R_p = 15 \rho_{iv}$, $L = 50 \rho_{iv}$. Note close agreement with Fig. 2. Topology checks marked by circles.

Figure 14 z plane, case I. $\beta_{\perp} = 0.86$, $\beta_{\parallel} = 0.474$, $\omega/\omega_{ci} = (0.3992,$
0.0000).

Figure 15 z plane, case I. $\beta_{\perp} = 0.94$, $\beta_{\parallel} = 0.534$, $\omega/\omega_{ci} = (0.3725,$
0.0000).

Figure 16 z plane, case I. $\beta_{\perp} = 0.99$, $\beta_{\parallel} = 0.568$, $\omega/\omega_{ci} = (0.1828,$
0.0000).

NOTICE

This report was prepared as an account of work sponsored by the United States Government. Neither the United States nor the United States Department of Energy, nor any of their employees, nor any of their contractors, subcontractors, or their employees, makes any warranty, express or implied, or assumes any legal liability or responsibility for the accuracy, completeness or usefulness of any information, apparatus, product or process disclosed, or represents that its use would not infringe privately-owned rights.

Reference to a company or product name does not imply approval or recommendation of the product by the University of California or the U.S. Department of Energy to the exclusion of others that may be suitable.

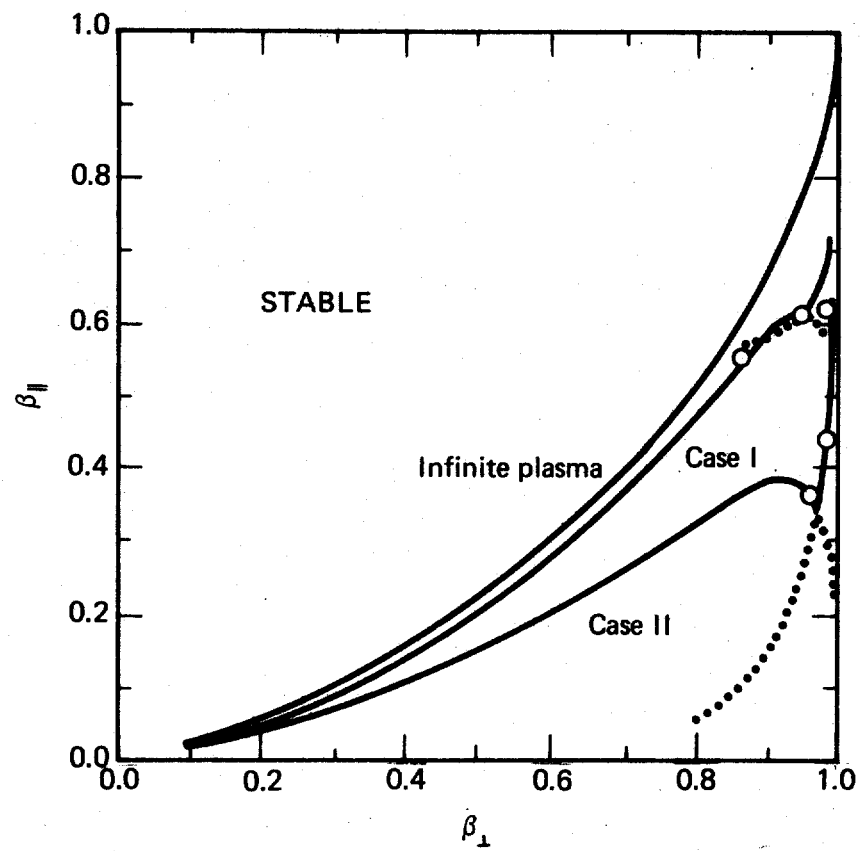


Fig. 1
Duncan C. Watson

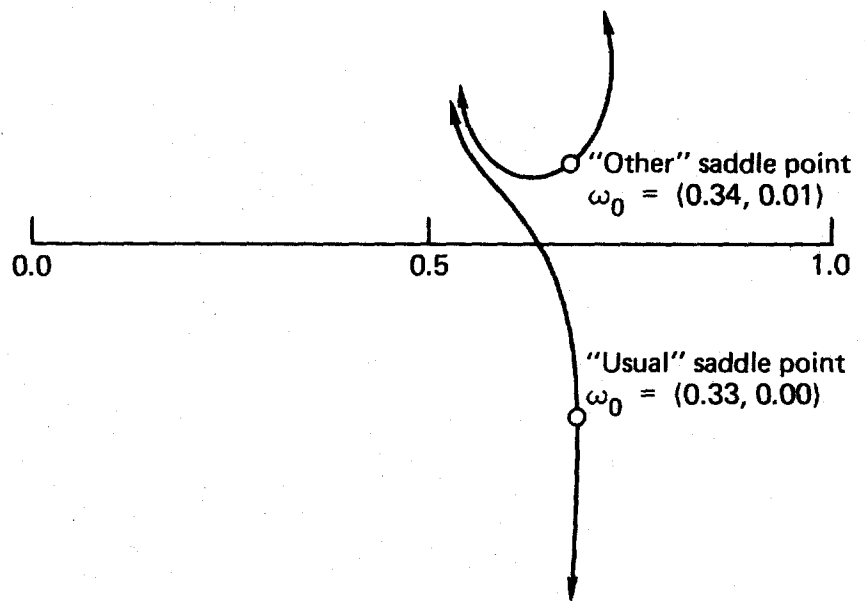


Fig. 2
Duncan C. Watson

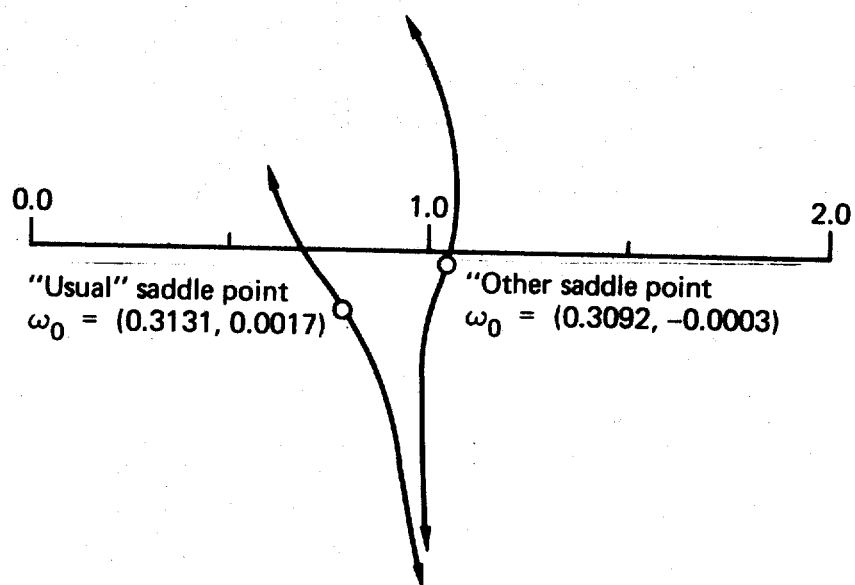


Fig. 3
Duncan C. Watson

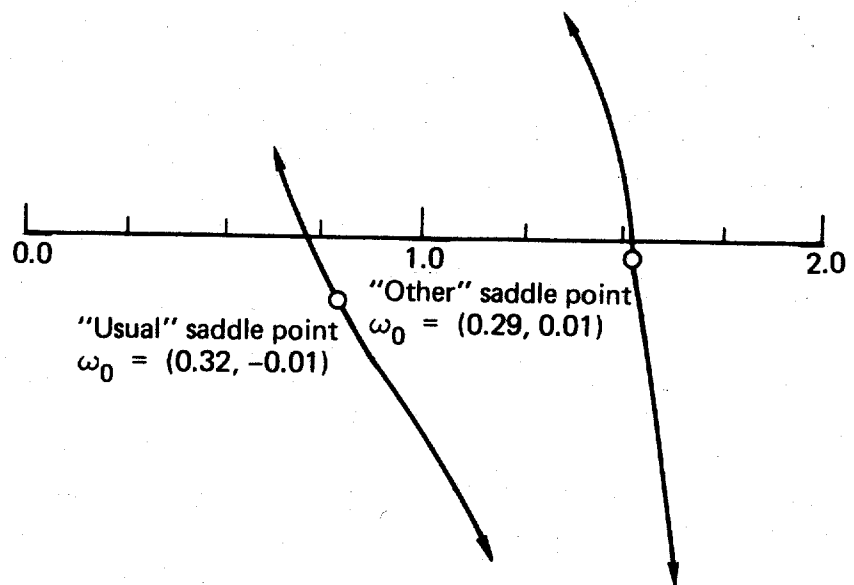


Fig. 4
Duncan C Watson

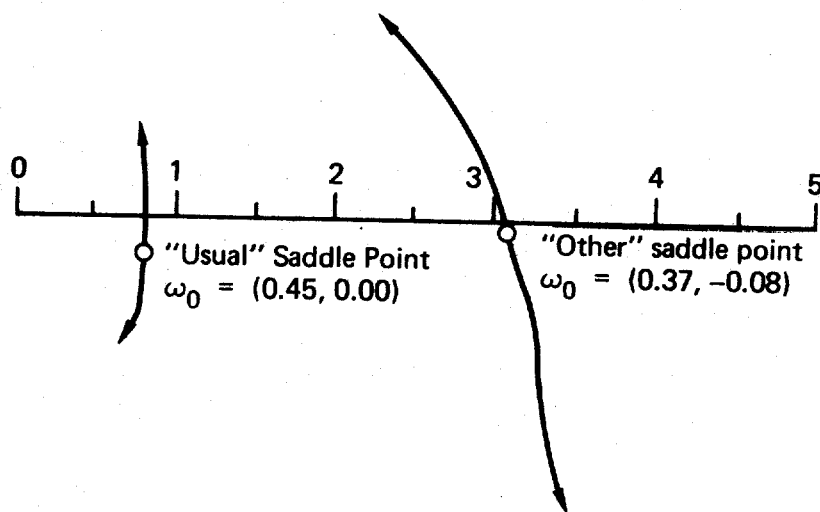


Fig. 5
Duncan C. Watson

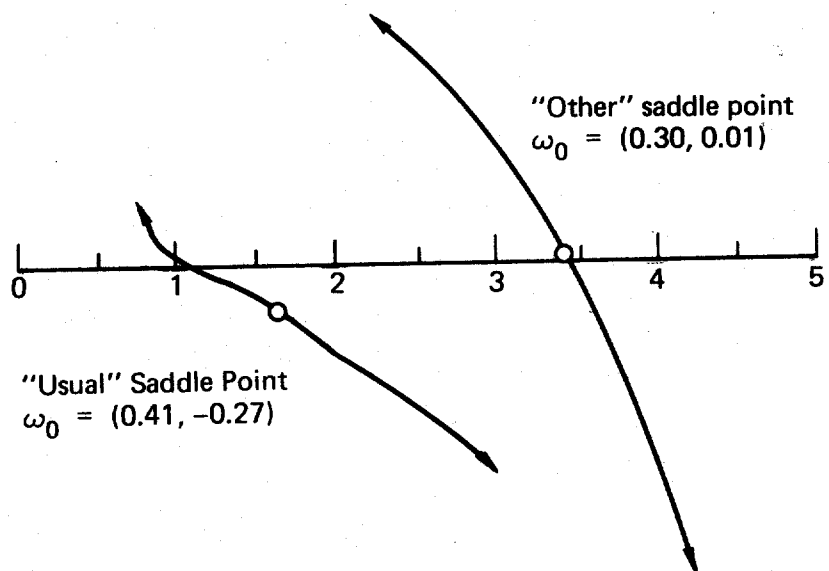


Fig. 6
Duncan C. Watson

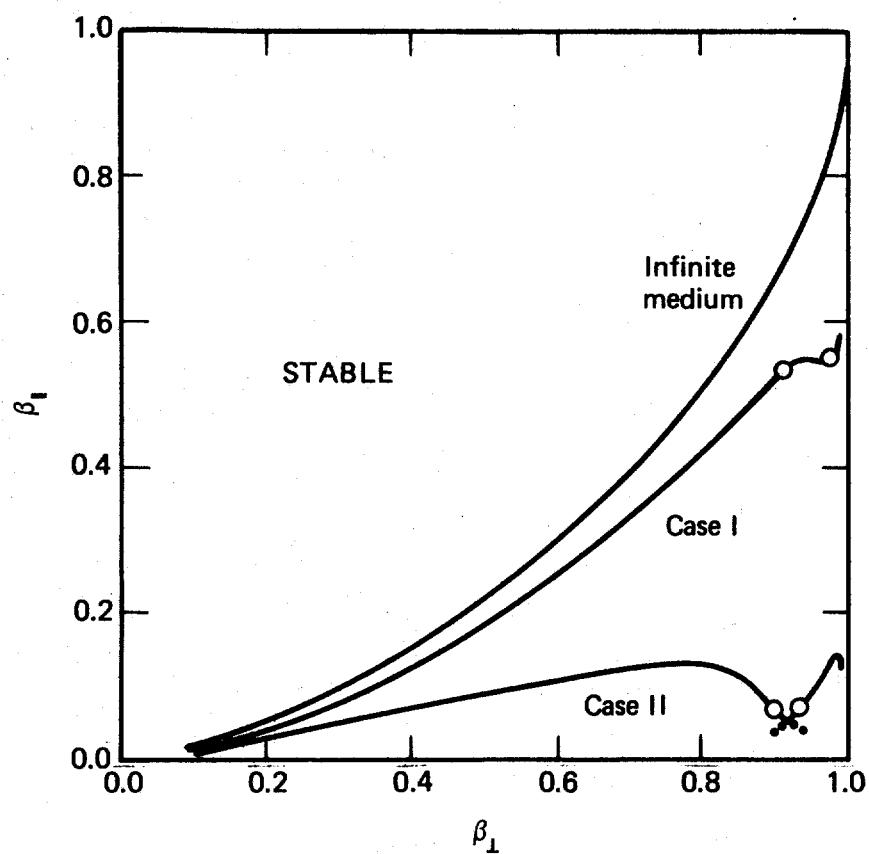


Fig. 7
Duncan C. Watson

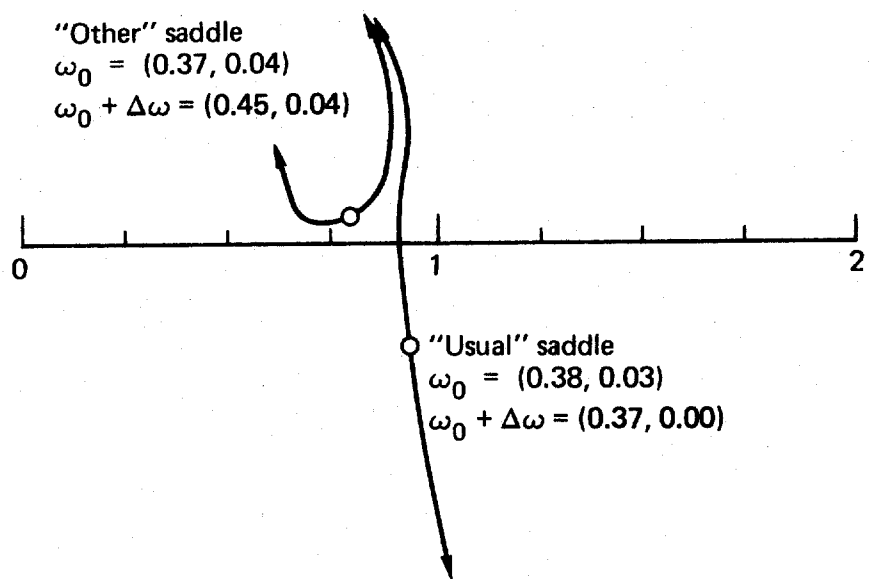


Fig. 8
Duncan C Watson

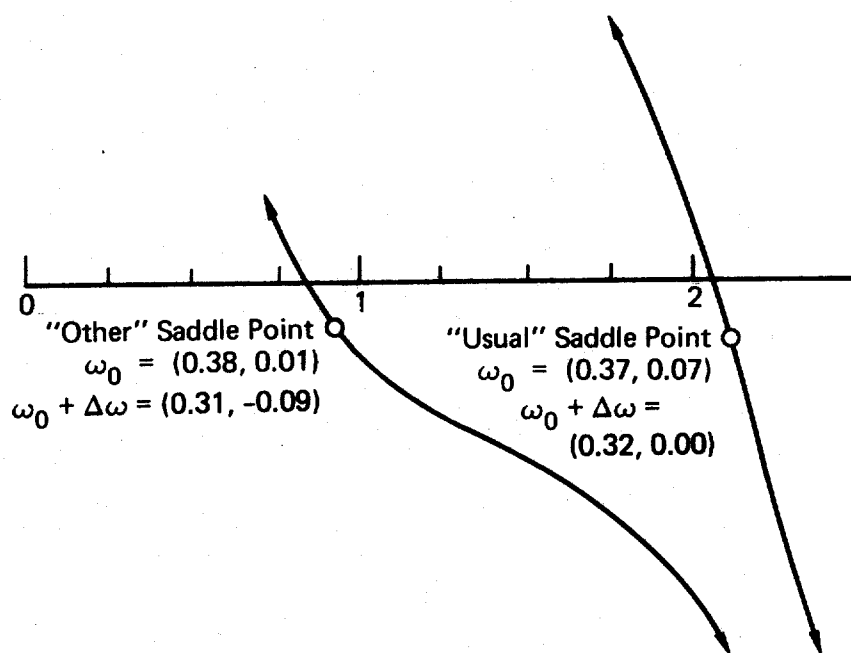


Fig. 9

Duncan C. Watson

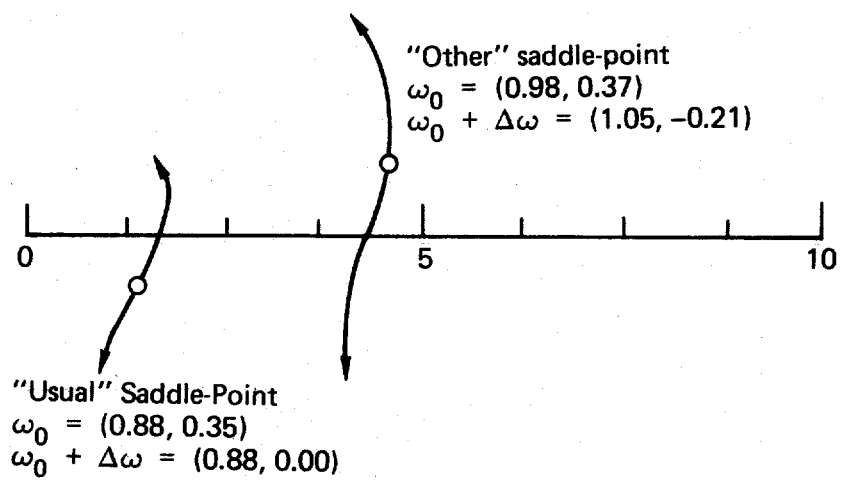


Fig. 10
Duncan C. Watson

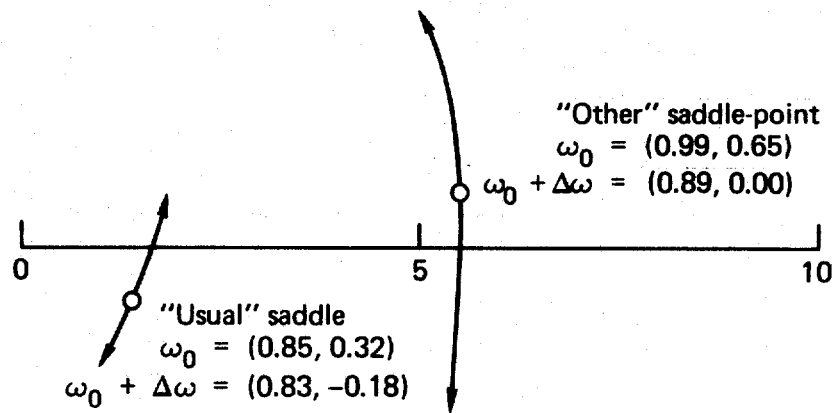


Fig. 11
Duncan C. Watson

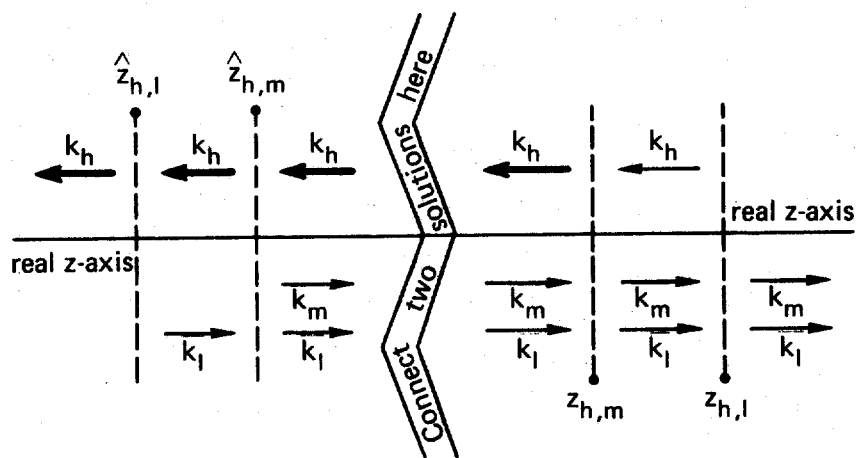


Fig. 12
Duncan C. Watson

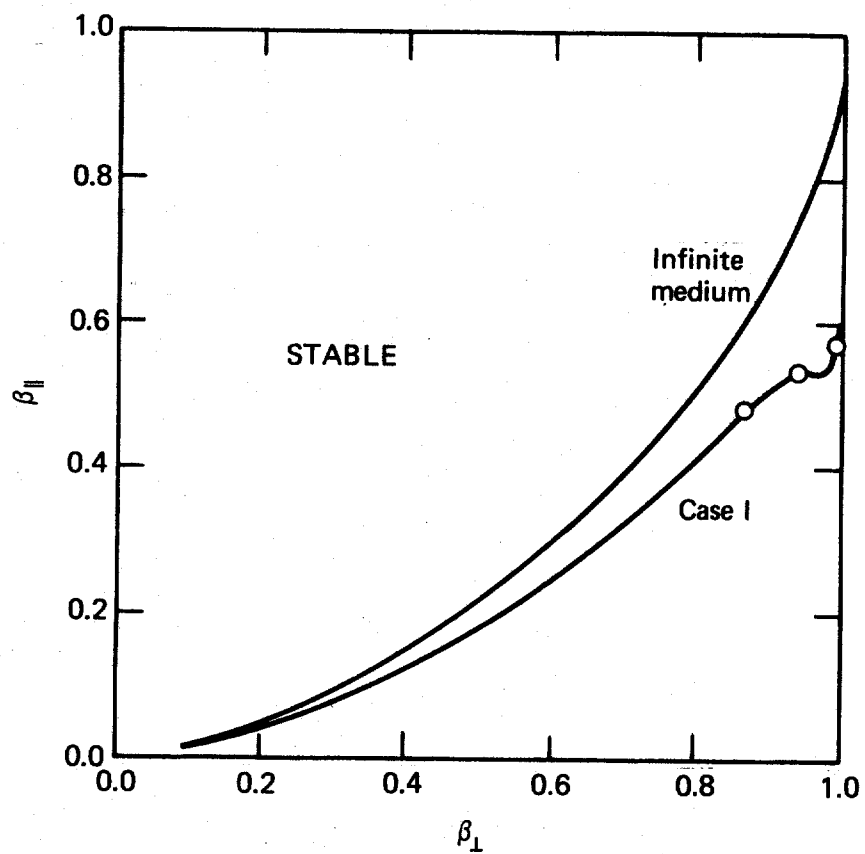


Fig. 13
Duncan C. Watson

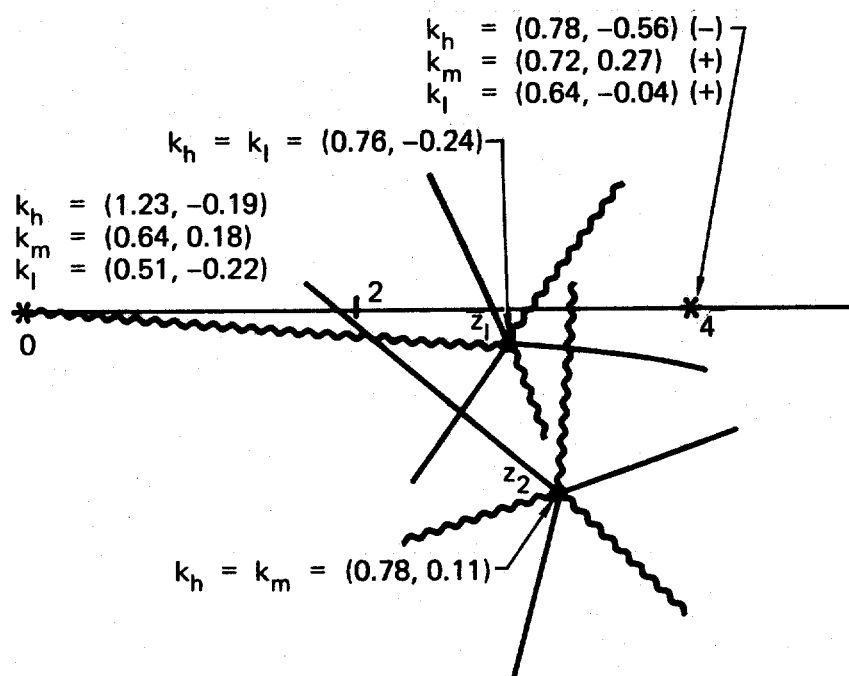


Fig. 14
Duncan C. Watson

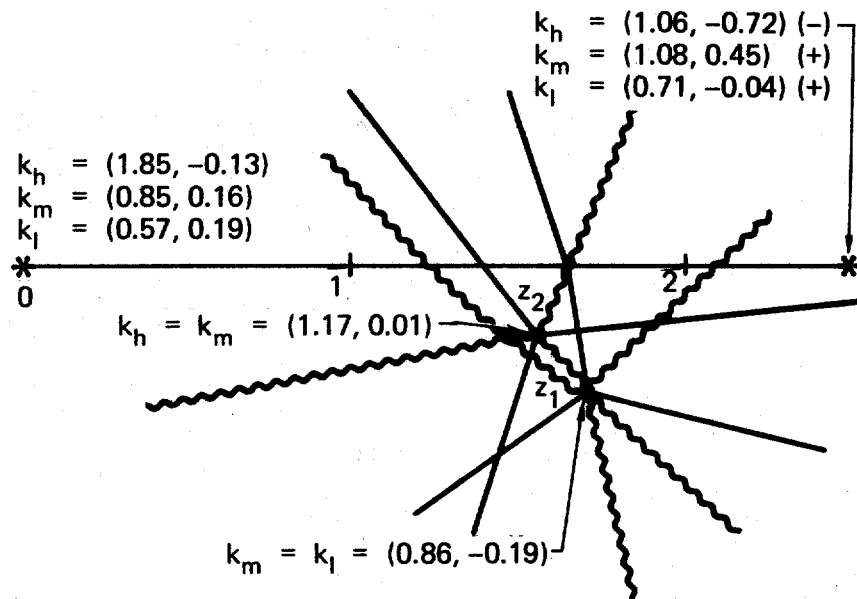


Fig. 15
Duncan C. Watson

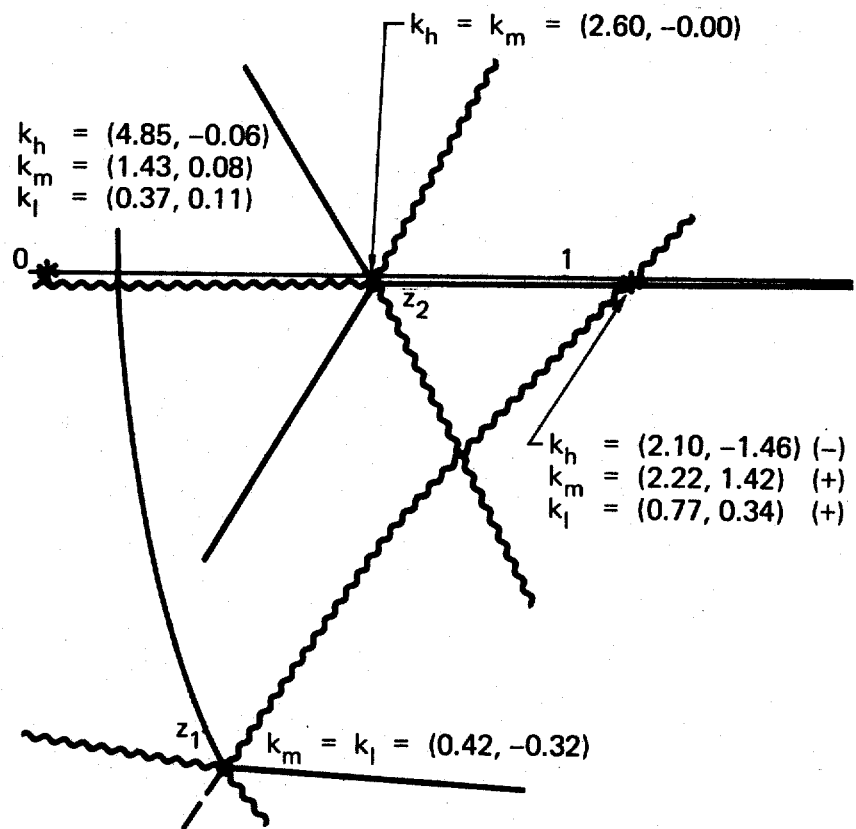


Fig. 16
Duncan C. Watson